The $\mathrm{sech}(\hat{\xi})$-type profiles: a Swiss-Army knife for exact analytical modeling of thermal diffusion and wave propagation in graded media

J.-C. Krapez

ONERA, The French Aerospace Lab, DOTA, F-13661 Salon de Provence, France

E-mail: jean-claude.krapez@onera.fr

Abstract

This work deals with the exact analytical modeling of transfer phenomena in heterogeneous materials exhibiting one-dimensional continuous variations of their properties. Regarding heat transfer, it has recently been shown that by applying a Liouville transformation and multiple Darboux transformations, infinite sequences of solvable profiles of thermal effusivity can be constructed together with the associated temperature (exact) solutions, all in closed-form expressions (vs. the diffusion-time variable and with a growing number of parameters). In addition, a particular class of profiles, so-called $\mathrm{sech}\left(\hat{\xi}\right)$-type profiles, exhibit high agility and at the same time parsimony. In this paper we delve further into the description of these solvable profiles and their properties. Most importantly, their quadrupole formulation is provided, enabling smooth synthetic profiles of effusivity of arbitrary complexity to be built, and allowing the corresponding temperature dynamic response to be obtained very easily thereafter. Examples are given with increasing variability of the effusivity and an increasing number of elementary profiles. These highly flexible profiles are equally relevant for providing an exact analytical solution to wave propagation problems in 1D graded media (i.e., Maxwell's equations, the acoustic equation, the telegraph equation, etc.). From now on, whether it be for diffusion-like or wave-like problems, when the leading properties present (possibly piecewise-) continuously heterogeneous profiles, the classical staircase model can be advantageously replaced by a "high-level" quadrupole model consisting of one or more $\mathrm{sech}\left(\hat{\xi}\right)$-type profiles, which makes the latter a true Swiss-Army knife for analytical modeling.

Keywords: Darboux Transformation; Depth-profiling; Effusivity profile; Graded properties; Liouville Transformation; Heterogeneous, Functionally Graded Material, Refractive Index, Diffusivity.

1 Introduction

Graded media are ubiquitous. Examples can be found at different scales, both in nature and in manmade materials. Living tissues (skin, teeth), wood, soils, rocks and the atmospheric boundary layer are common examples. In manmade materials, the gradient structure may appear incidentally (for instance, due to matter diffusion), whereas in functionally graded materials (FGM) it is introduced on purpose to achieve target properties. In a first instance, the gradient affects composition, microstructure or porosity [1]; some examples are: fiber-reinforced layered composites, ceramic thermal barriers, case-hardened steels, and armor plates.

Difficulties arise when studying diffusion processes (e.g., heat diffusion) inside continuously heterogeneous media because, even for the one-dimensional (1D) case, an exact general (closed-form) solution is lacking for *arbitrary profiles* of the leading parameters. One remedy consists in approximating these profiles; another consists in approximating the transfer equation. In the first case, when the profiles are not too complex, one can try to approach them with profiles leading to known temperature analytical solutions. Examples are linear [2], power-law [2, 3], and exponential [3-5] profiles of the conductivity or the specific heat, as well as trigonometric and hyperbolic profiles of the square root of conductivity [6]. In specifically transformed spaces, exponential [7, 8] and power law [9] profiles of effusivity also yield explicit closed-form solutions. The disadvantage for many of them is that they require the use of special functions (e.g., Bessel, Airy, hypergeometric functions, etc.), which penalizes the computation time, especially when the temperature data have to be calculated iteratively, as for example in the core of an inversion routine. Profiles presenting more complex shapes require other strategies to be implemented, such as an approximation with staircase functions [10, 11] or with piecewise-linear functions [5, 12-15]. Obviously, the finer the spatial discretization, the better the results [12, 15].

The second approach (i.e., approximation of the heat equation) consists in applying a perturbation method [16], a linearization of the non-linear differential equation describing the variations of the thermal reflection coefficient [17-18] or thermal impedance [19], the WKBJ method [20], or an empirical method [21] derived from the THO theory, whose result is closely related to the latter. All of these methods require the thermal properties to have small and slow variations with position.

A third group of methods is based on a series expansion of the solution: the Generalized Integral Transform method [22], the Spectral Parameter Power Series method [23] and an asymptotic expansion for thermal waves at high frequency [24]. All may admit arbitrary profiles of the thermal properties as input data (provided some integrability or derivability criteria are met), however, since the temperature solution involves infinite series,

which unavoidably have to be truncated, these methods should also be considered approximate (in addition, the required number of terms in the series depends on the steepness of the profiles).

A method was described a few years ago for building sequences of *solvable profiles* for several types of transfer equations in graded materials, in particular the heat equation and the wave equation [25] (a *solvable profile* means a profile of the leading property for which an exact analytical expression of the thermal field or wave field solution can be found). The underlying technique is the Bäcklund transformation applied in the time domain. Recently, we presented a simpler method, the PROFIDT method (PROperty and FIeld Darboux Transformation), which is equally efficient for diffusion equations (like the heat equation) [26, 27] and for wave equations (like Maxwell's equations describing electromagnetic (EM) wave propagation in lossless and source-free media with graded permittivity and permeability) [28]. In both cases, it should be applied in the Laplace domain or Fourier domain (in these domains, all solutions presented in [26-28] are in closed-form; some are in closed-form even after getting back in the time domain [27]). The PROFIDT method can be iterated to produce increasingly sophisticated solvable profiles of the leading property (namely, thermal effusivity for the thermal problem and the EM tilted admittance for the EM-wave problem) together with the field solution (temperature or heat flux field, resp. electric or magnetic field). Another option is to use intermediate-order solvable profiles (that is, obtained after applying one single PROFIDT) and merge them; the dynamic response of the whole heterogeneous structure is then obtained by applying the transfer matrix method and multiplying the quadrupoles related to each elementary profile, as for any passive multilayer [29, 30]. A family of profiles has proved particularly interesting for this purpose; they were called "$\operatorname{sech}\left(\hat{\xi}\right)$-type" profiles. They are defined with four parameters and those can be adjusted so that the values of the modeled property at both ends of a given layer, together with its first derivatives, reach any set of four specified (finite) values. By taking advantage of this flexibility, it was envisioned that smooth solvable profiles of any shape could be synthesized by assembling elementary profiles of $\operatorname{sech}\left(\hat{\xi}\right)$-type.

In this work, we aim to build upon the previous study and provide a thorough investigation and exploration of the properties of this special class of solvable profiles. Our goal is to advance the state of the art by developing effective analytical tools for modeling diffusion processes, as well as wave propagation in complex media described by a 1D continuously heterogeneous distribution of their properties.

To present the approach and outcomes, this paper is organized as follows. In Section 2, the main principles of the PROFIDT method are briefly recalled. In Section 3, the $\operatorname{sech}\left(\hat{\xi}\right)$-type profile definition is reported, followed by a presentation of their properties. In Section 4, we describe the tools necessary for applying the quadrupole

methodology in the context of $\mathrm{sech}(\hat{\xi})$-type heterogeneity. Examples with gradual complexity and relevant to modulated photothermal experiments are presented in Section 5. Finally, Section 6 is a discussion on applications to other kinds of problems, like wave propagation in media with continuously heterogeneous wave celerity, in particular light transmission in dielectrics with graded refractive index.

2 Fundamentals of the PROFIDT method [26]

Let us consider 1D heat diffusion in a medium with graded thermal conductivity $\lambda(z)$ and graded volumetric heat capacity $c(z)$. A Laplace transformation (or a Fourier transformation) is first applied, which changes temperature $T(z,t)$ into $\theta(z,p)$ and heat flux density $\varphi(z,t)$ into $\phi(z,p)$, where the variable p stands for either the Laplace variable (transient regime) or the Fourier variable $i\omega$, where ω is the angular frequency $2\pi f$ (periodic regime). The heat equation is usually expressed in terms of temperature (we will then use the symbol $\langle T \rangle$):

$$\langle T \rangle : \qquad p\theta = \frac{1}{c(z)} \frac{d}{dz}\left(\lambda(z) \frac{d\theta}{dz} \right) \tag{1}$$

A similar equation can be found for the heat flux density $\phi = -\lambda\, d\theta/dz$, where, remarkably enough, $\lambda(z)$ and $c^{-1}(z)$ are simply interchanged with respect to the previous one (the symbol $\langle \varphi \rangle$ will be used for all features related to this second equation):

$$\langle \varphi \rangle : \qquad p\phi = \lambda(z) \frac{d}{dz}\left(\frac{1}{c(z)} \frac{d\phi}{dz} \right) \tag{2}$$

A Liouville transformation is then applied. The first step consists in changing the *independent* variable z (i.e., the physical depth) into the *square root of the diffusion time* (SRDT) ξ, which is defined from the diffusivity profile $a(z) = \lambda(z)/c(z)$ according to (the same origin is taken for both z-scale and ξ-scale):

$$\xi = \int_0^z a^{-1/2}(u)\, du \tag{3}$$

The second step consists in changing the *dependent* variable, either the temperature (in Eq. (1)) or the heat flux (in Eq. (2)), into a new one (invariably written $\psi(\xi, p)$) by multiplying the former by a function $s(\xi)$ that is related to the thermal effusivity profile $b(z) = \sqrt{\lambda(z) c(z)}$ in two different ways depending on the considered form, $\langle T \rangle$ or $\langle \varphi \rangle$:

$$\langle T \rangle : \qquad \theta(\xi, p) \to \psi(\xi, p) \equiv \theta(\xi, p) s(\xi); \quad s(\xi) \equiv b^{+1/2}(\xi) \tag{4}$$

$$\langle \varphi \rangle : \qquad \phi(\xi, p) \to \psi(\xi, p) \equiv \phi(\xi, p) s(\xi); \quad s(\xi) \equiv b^{-1/2}(\xi) \tag{5}$$

In either case, substituting this new dependent variable $\psi(\xi, p)$ in Eq. (1) resp. in Eq. (2), leads to a 2nd order ODE in the so-called Liouville normal form [31], i.e., $\psi'' = (V(\xi) + p)\psi$ (from now on, a prime denotes a derivation with respect to ξ). Interestingly, in either case, the function $V(\xi)$ corresponds to the ratio $s''(\xi)/s(\xi)$. This new equation is actually equivalent to a stationary Schrödinger equation in which the function $V(\xi) = s''(\xi)/s(\xi)$ plays the role of the "potential" function. First, this tells us the paramount importance of the effusivity profile when modeling 1D dynamic heat transfer in graded media. Next, this particular form of potential has the very interesting consequence that each of the former Schrödinger equations can be split into a system of two homologous Schrödinger equations, which means equations sharing the same potential function $V(\xi)$. The first one, with the variable p acting as an eigenvalue, is for the "field" function $\psi(\xi, p)$; the second one, with a vanishing eigenvalue, is for the "property" function $s(\xi)$:

$$\begin{cases} \psi'' = (V(\xi) + p)\psi & \text{(6a)} \\ s'' = V(\xi)s & \text{(6b)} \end{cases}$$

The problem comes down to seeking solvable profiles $V(\xi)$ for the general Schrödinger equation (6a) with arbitrary value of the constant parameter p. Obviously, in addition to solutions for $\psi(\xi, p)$ in Eq. (6a), this would simultaneously provide solutions for $s(\xi)$ in Eq. (6b) as a particular case of Eq. (6a) with $p = 0$. Then, by using it in the reverse order Eq. (4) or (5) (as appropriate), one concomitantly obtains the temperature field (or the heat flux field) and the associated effusivity profile, all in generic forms.

To start with, simple analytical solutions for $b^{+1/2}(\xi)$ or $b^{-1/2}(\xi)$ can be obtained by choosing a constant value for the potential function $V(\xi)$. Positive (or negative) values yield linear combinations (LC) of hyperbolic (resp. trigonometric) functions of a scaled SRDT. On the other side, a nil potential gives rise to linear functions of ξ.

The Darboux transformation is a perfect method for enriching the previous solutions. This is a differential transformation that, given the general solution of Eq. (6a) with a solvable profile $V_0(\xi)$ and one particular solution, provides a new solvable profile $V_1(\xi)$ and the general solution of Eq. (6a), with $V(\xi) = V_1(\xi)$. This was the first time, in [26], for heat-like equations and in [28], for wave-like equations, that the Darboux transformation was applied in tandem to find new solvable profiles of the leading property (effusivity in the first case, EM admittance in the second case) and the related analytical closed-form expression of the diffusion or wave fields. The joint procedure was dubbed the PROFIDT method (PROperty and FIeld Darboux Transformation method). In addition, the PROFIDT method can be applied iteratively to obtain increasingly

sophisticated solutions [26, 28]. As a matter of fact, at each step, the new set of effusivity profiles is enriched with up to two parameters.

We will now concentrate on a specific class of solvable profiles, the so-called $\mathrm{sech}\left(\hat{\xi}\right)$-type profiles. These have been generated by a single Darboux transformation, starting from a constant positive potential function.

3 The $\mathrm{sech}\left(\hat{\xi}\right)$–type profiles

3.1 Description in the (square-root) diffusion-time space (i.e., ξ-space)

They are defined as a linear combination of two linearly independent solutions of Eq. (6b), $B(\xi)$ and $D(\xi)$, with the potential $V(\xi)=\xi_c^{-2}\left(1-2\,\mathrm{sech}\left(\hat{\xi}\right)\right)$:

$$\begin{cases} B(\xi)=\mathrm{sech}\left(\hat{\xi}\right) \\ D(\xi)=\sinh\left(\hat{\xi}\right)+\hat{\xi}\,\mathrm{sech}\left(\hat{\xi}\right) \end{cases} \tag{7}$$

The function sech is the inverse of the hyperbolic cosine: $\mathrm{sech}=1/\cosh$. $\hat{\xi}$ is the result of a linear transformation of the SRDT, ξ, namely $\hat{\xi}=\xi/\xi_c+\tau$. It involves two free-parameters: ξ_c (a characteristic SRDT) and τ that may take values in $]0,+\infty[$, resp. in $]-\infty,+\infty[$. With A_B and A_D, two other free parameters, the effusivity profiles are written as:

$$b^{\pm 1/2}(\xi)=s(\xi)=A_B B(\xi)+A_D D(\xi) \tag{8}$$

The "$+1/2$" exponent in Eq. (8) refers to profiles originating from the $\langle T\rangle$-form heat equation and "$-1/2$" to those originating from the $\langle\varphi\rangle$-form equation. Two sub-classes can thus be generated, according to the exponent sign. The effusivity profiles in Eq. (8) are defined with *four* adjustable parameters: ξ_c, τ and the two multiplicative factors A_B and A_D. It was shown in [26] that the profiles generated from the LC in Eq. (8) are highly flexible functions: they may be concave, convex or wavy and they exhibit arbitrary steepness at the layer boundaries. Indeed, over a given ξ-interval, any *four* boundary conditions set can be satisfied, namely two end-values for $s(\xi)$ (non-zero and finite values) and two others for its derivative (finite values). At the same time, they exhibit maximum parsimony in satisfying these conditions, since they are defined with *no more than four* parameters. For these reasons, the "$\mathrm{sech}\left(\hat{\xi}\right)$-type" profiles are expected to be quite efficient for fitting any target profile, if needed, by assembling two or more of them.

Simultaneously with the $s(\xi)$ function in Eq. (8), the PROFIDT method provided the associated field function $\psi(\xi,p)$ through a LC of two functions $K(\xi,p)$ and $P(\xi,p)$:

$$\psi(\xi,p)=A_K K(\xi,p)+A_P P(\xi,p) \tag{9}$$

which are defined by:

$$\begin{cases} K(\xi,p) \equiv \alpha S(\xi,p) - \sigma C(\xi,p) \\ P(\xi,p) \equiv \alpha C(\xi,p) - \sigma S(\xi,p) \end{cases} \tag{10}$$

with:

$$\begin{cases} C(\xi,p) \equiv \cosh(\alpha\xi) \\ S(\xi,p) \equiv \sinh(\alpha\xi) \end{cases}; \qquad \begin{cases} \sigma = \sigma(\xi) \equiv \xi_c^{-1} \tanh\left(\hat{\xi}\right) \\ \alpha = \alpha(p) \equiv \sqrt{p + \xi_c^{-2}} \end{cases} \tag{11}$$

3.2 Back to the (real) depth-space (i.e., z-space)

The PROFIDT method yields effusivity (solvable) profiles and temperature analytical solutions that are defined in Liouville space, i.e., in ξ-space. Under some circumstances, it may be necessary to have a description of these in the z-space as well. The simplest case is when the diffusivity profile $a(z)$ is known; this implies that ξ is substituted in the effusivity or temperature expression by $\xi(z)$, which is calculated from Eq. (3) by incorporating the expression $a(z)$. The trivial case of a constant diffusivity ($a(z) = a_=$) leads to $\xi(z) = z/\sqrt{a_=}$. Other cases were described in [26]; one of them yields an *implicit* description of the effusivity profile through the coupled relations:

$$\begin{cases} b = b(\xi) \\ z = z(\xi) \end{cases} \tag{12}$$

where $z(\xi)$ is obtained by inverting Eq. (3), which amounts to a Liouville *inverse transformation*. To be effective, this inversion requires extra information on the diffusivity, volumetric heat capacity or conductivity. Knowing that the inverse of Eq. (3) may take the following equivalent forms:

$$z = z(\xi) = \int_0^\xi \sqrt{a(u)}\,du = \int_0^\xi \frac{b(u)}{c(u)}\,du = \int_0^\xi \frac{\lambda(u)}{b(u)}\,du \tag{13}$$

the extra information that either volumetric heat capacity or conductivity is constant (i.e., $c(z) = c_=$ or $\lambda(z) = \lambda_=$) allows the latter two quadratures to be simplified. A constant volumetric heat capacity (this hypothesis is generally adopted when dealing with condensed phases, such as, for example, case hardened steel) would imply calculating the primitive of effusivity in the ξ-space. A constant conductivity (a situation that is less often met) would imply calculating the primitive of its inverse. Analytical expressions of these primitives were proposed in [26] for $\mathrm{sech}\left(\hat{\xi}\right)$-type profiles, which can be summarized in a set of four equations:

$$z(\xi) = \frac{\xi_c}{c_=}\left[f\left(\hat{\xi}(\xi)\right) - f\left(\hat{\xi}(0)\right)\right] \qquad \text{for } c(z) = c_= \tag{14}$$

$$z(\xi) = \xi_c \lambda_= \left[f\left(\hat{\xi}(\xi)\right) - f\left(\hat{\xi}(0)\right)\right] \qquad \text{for } \lambda(z) = \lambda_= \tag{15}$$

$$f\left(\hat{\xi}\right) = A_B{}^2 \tanh\left(\hat{\xi}\right) + A_D{}^2\left[\frac{1}{4}\sinh\left(2\hat{\xi}\right) - \frac{\hat{\xi}}{2} + \hat{\xi}^2 \tanh\left(\hat{\xi}\right)\right] + 2A_B A_D \hat{\xi} \tanh\left(\hat{\xi}\right) \tag{16}$$

$$f\left(\hat{\xi}\right)=\begin{cases}\dfrac{-1}{2A_D}\dfrac{\operatorname{sech}\left(\hat{\xi}\right)}{b^{\pm 1/2}\left(\hat{\xi}\right)} & \text{if} \quad A_D \neq 0 \\ \dfrac{1}{2A_B}\dfrac{\sinh\left(\hat{\xi}\right)+\hat{\xi}\operatorname{sech}\left(\hat{\xi}\right)}{b^{\pm 1/2}\left(\hat{\xi}\right)} & \text{if} \quad A_B \neq 0\,.\end{cases} \tag{17}$$

Eq. (16) should be used in the case of $\langle T\rangle$-form profiles and constant heat capacity (with Eq. (14)) or in the case of $\langle\varphi\rangle$-form profiles and constant conductivity (with Eq. (15)). On the other side, Eq. (17) should be used in the case of $\langle T\rangle$-form profiles (by selecting the positive exponent for effusivity at the denominator) and constant conductivity (with Eq. (15)), or in the case of $\langle\varphi\rangle$-form profiles (by selecting the negative exponent) and constant heat capacity (with Eq. (14)).

Furthermore, one can notice that Eq. (13) could also be written in the following form:

$$z=\int_0^{\xi}\lambda^q(u)c^{q-1}(u)b^{1-2q}(u)du \tag{18}$$

where q is a constant real number. If $\lambda^q(z)c^{q-1}(z)$ happened to be constant for a particular value of q, Eq. (18) would amount to calculating the primitive of $b^{1-2q}(\xi)$. Except for very special cases ($q=0$, $q=1/2$, and $q=1$ correspond to the previous cases of constant $c(z)$, constant $a(z)$ and constant $\lambda(z)$), this would require a numerical computation of this quadrature.

4 Tools for implementing the quadrupole methodology

Useful relations regarding both $\langle T\rangle$-form and $\langle\varphi\rangle$-form profiles are first recalled [26]:

$$\langle T\rangle:\ \begin{cases}b=s^2\\ \theta=\psi\, s^{-1}\\ \phi=-W(s,\psi)\end{cases}\qquad \langle\varphi\rangle:\ \begin{cases}b=s^{-2}\\ \theta=-p^{-1}W(s,\psi)\\ \phi=\psi\, s^{-1}\end{cases} \tag{19}$$

where W is the Wronskian: $W(s,\psi)=s\psi'-s'\psi$.

The quadrupole (or transfer) matrix $\mathbf{M}$ of a layer extending from $z=z_0$ to $z=z_1$ (i.e., from $\xi=\xi_0$ to $\xi=\xi_1$ in ξ–space; in the sequel, 0 or 1 index means that the functions are evaluated at ξ_0, resp. at ξ_1) relates the input temperature/heat flux vector, i.e., $[\theta_0 \quad \phi_0]^t$, to the output vector, i.e., $[\theta_1 \quad \phi_1]^t$, as follows (see e.g., [29, 30]):

$$\begin{bmatrix}\theta_0\\ \phi_0\end{bmatrix}=\mathbf{M}\cdot\begin{bmatrix}\theta_1\\ \phi_1\end{bmatrix} \tag{20}$$

Quadrupoles $\mathbf{M}_{\langle T\rangle}$ and $\mathbf{M}_{\langle\varphi\rangle}$ are obtained when considering profiles of $\langle T\rangle$-form, resp. of $\langle\varphi\rangle$-form. Their calculation follows the classical procedure described, for instance, in [29, 30]. Hence, a synthetic expression for $\mathbf{M}_{\langle T\rangle}$ is given by:

$$\mathbf{M}_{\langle T\rangle}=\begin{bmatrix} K/s & P/s \\ -W(s,K) & -W(s,P)\end{bmatrix}_0\times\begin{bmatrix} K/s & P/s \\ -W(s,K) & -W(s,P)\end{bmatrix}_1^{-1} \tag{21}$$

After some algebra, the four terms of the matrix are expressed as follows:

$$\mathbf{M}_{\langle T\rangle}=\begin{bmatrix} A & B \\ C & D\end{bmatrix}=\frac{1}{\Delta}\begin{bmatrix} s_0^{-1}s_1(G-\mu_1 I) & s_0^{-1}s_1^{-1}I \\ -s_0s_1(-\mu_0 G-\mu_1 H+\mu_0\mu_1 I+J) & s_0s_1^{-1}(-H+\mu_0 I)\end{bmatrix} \tag{22}$$

where μ_0, μ_1 correspond to the values taken by the relative derivative: $\mu_{0,1}=s_{0,1}{}'/s_{0,1}$ on both sides of the layer. The terms G, H, I, J, Δ involve the values taken at the two layer edges by the independent functions $K(\xi,p)$ and $P(\xi,p)$ and by their derivatives:

$$\begin{cases} G=K_0P_1{}'-K_1{}'P_0 & H=K_0{}'P_1-K_1P_0{}' \\ I=K_0P_1-K_1P_0 & J=K_0{}'P_1{}'-K_1{}'P_0{}' \\ \Delta=W(K,P)=K_1P_1{}'-K_1{}'P_1=K_0P_0{}'-K_0{}'P_0 & \end{cases} \tag{23}$$

We now build upon the previous study and provide useful expressions for the $\mathrm{sech}(\hat{\xi})$-profile case. When taking into account the expressions of $K(\xi,p)$ and $P(\xi,p)$ in Eq. (10)-(11), we obtain $\Delta=-\alpha p$ and:

$$\begin{bmatrix} G \\ H \\ I \\ J\end{bmatrix}=-\begin{bmatrix} \sigma_1(\sigma_1-\sigma_0)+p & \sigma_0 p-\sigma_1(\alpha^2-\sigma_0\sigma_1) \\ \sigma_0(\sigma_1-\sigma_0)-p & \sigma_1 p-\sigma_0(\alpha^2-\sigma_0\sigma_1) \\ -(\sigma_1-\sigma_0) & \alpha^2-\sigma_0\sigma_1 \\ (\sigma_1-\sigma_0)(p-\sigma_0\sigma_1) & \alpha^2\sigma_0\sigma_1-(\sigma_0{}^2+p)(\sigma_1{}^2+p)\end{bmatrix}\times\begin{bmatrix} \alpha\cosh(\alpha\xi_1) \\ \sinh(\alpha\xi_1)\end{bmatrix} \tag{24}$$

The construction of the $\mathbf{M}_{\langle\varphi\rangle}$ matrix is just slightly different. A careful analysis of Eq. (19) shows that, except for the presence of p^{-1}, the roles of the temperature and heat flux are interchanged in the second and third line between the $\langle T\rangle$-form and $\langle\varphi\rangle$-form expressions. This means that once the right hand side of Eq. (22) has been computed by substituting the proper values of α s_0, s_1, μ_0, μ_1 σ_0 and σ_1 (i.e., those relevant for the $\langle\varphi\rangle$-form profile), these four entries *A, B, C, D* provide the four entries of the $\mathbf{M}_{\langle\varphi\rangle}$ matrix according to:

$$\mathbf{M}_{\langle\varphi\rangle}=\begin{bmatrix} D & p^{-1}C \\ pB & A\end{bmatrix} \tag{25}$$

Thus, both matrices $\mathbf{M}_{\langle T\rangle}$, in Eq. (22), and $\mathbf{M}_{\langle\varphi\rangle}$, in Eq. (25), are aimed at operating on vectors constituted by temperature and heat flux that are arranged in the same order: viz. $[\theta \quad \phi]^t$; see Eq. (20). By doing so, multilayers of mixed type, i.e., $\langle T\rangle$-form and $\langle\varphi\rangle$-form, can be easily simulated; one just has to multiply transfer matrices like Eq. (22), resp. Eq. (25), in due order.

All ingredients have now been provided for the computation of the transfer matrices related to the $\mathrm{sech}(\hat{\xi})$-type profiles. The procedure for performing the calculation is outlined thereafter:

1- specify four boundary conditions on effusivity $b(\xi)$ and its derivative at the left-end and right-end of the graded layer : $b_0, b_1, b_0{}', b_1{}'$;

2- choose between the $\langle T\rangle$-form and the $\langle\varphi\rangle$-form;

3- translate the specifications on the derivatives of effusivity into specifications on the derivatives of $s(\xi)$ with reference to Eq. (8), while considering the appropriate $+1/2$ or $-1/2$ exponent;

4- identify the four parameters A_B and A_D, ξ_c and τ, such that $s(\xi)$ in Eq. (7)-(8) satisfies the four boundary conditions (specified values for s_0, s_1, s_0', s_1');

5- the whole profile $b(\xi)$ can then be drawn from Eq. (8) (by using Eq. (7)); the profile in z-space can be calculated from the appropriate equations in Eq. (14)-(17), depending on the form ($\langle T \rangle$ or $\langle \varphi \rangle$) and the underlying hypothesis (constant $c(z)$ or constant $\lambda(z)$);

6- for a given p Laplace-Fourier parameter, compute $\alpha(p)$ and the values of $\sigma(\xi)$ at both boundaries, σ_0 σ_1, from Eq. (11). Calculate the four quadrupole entries by computing the terms in Eq. (24) and substituting them into Eq. (22) and then, if appropriate, into Eq. (25).

The quadrupole matrix relevant of an association of $\mathrm{sech}(\hat{\xi})$-type profiles is naturally obtained by multiplying the individual matrices together.

At Step No. 2, the decision between the $\langle T \rangle$-form or the $\langle \varphi \rangle$-form may be motivated differently according to the situation. If an effusivity profile is given as a starting point and it simply needs to be modeled with a $\mathrm{sech}(\hat{\xi})$ -type profile, the decision will be in favor of the form that most closely matches it, whether in the ξ-space or in the z-space, as can be checked at the end of Step 5 (see, e.g., Figures 1 and 2 below). Another situation is thermal inversion where temperature measurements are provided and from which one seeks to recover the "hidden" (i.e., unknown) effusivity profile. The decision will then be in favor of the form, $\langle T \rangle$ or $\langle \varphi \rangle$, that leads to the temperature values that most closely match the input data. As such, the whole procedure, from Step 3 to Step 6, should be performed for both forms. Consequently, if the considered graded material is modeled with a stacking of N $\mathrm{sech}(\hat{\xi})$-type profiles, there is a possibility of 2^N combinations by selecting either the $\langle T \rangle$-form or the $\langle \varphi \rangle$-form for each elementary profile.

5 Applications

5.1 Simple examples: graded coatings

Fig. 1 is an illustration of $\mathrm{sech}(\hat{\xi})$-type profiles that adds to those already presented in [26, 28]. Those presented here are intended to represent a graded coating. Both $\langle T \rangle$-form and $\langle \varphi \rangle$-form profiles are reported (in plain, resp. dashed curves). We hypothesized a doubling in effusivity from b_0, at the left-end of the coating (free-surface), to b_1 at the right-end. We set a zero derivative at the right-end, whereas the derivative was given the values 2, -1.5, or 0 (normalized derivative $\xi_1 (b')_0 / b_0$) at the left-end. Respectively, the effusivity profiles show

an overshoot, an undershoot or they rise monotonically to the right-end value. In the latter case, the $\langle T \rangle$-form and $\langle \varphi \rangle$-form profiles are very similar, whereas in the former cases they are quite different, which highlights the interest in considering both $\langle T \rangle$-form and $\langle \varphi \rangle$-form options: this enriches quite simply the family of solvable profiles and offers the opportunity of choosing from many more forms in the modeling process.

The representation of these $\mathrm{sech}(\hat{\xi})$-type profiles in the (real) depth space is given in Fig. 2. Two hypotheses were considered: constant volumetric heat capacity (left plot) and constant heat conductivity (right plot). Notice that the case of constant diffusivity is, of course, already represented in Fig. 1, since z and ξ are then simply proportional. In the left plot of Fig. 2 a stretching or compression of the initial ξ-profile in Fig. 1 can be observed in those places where it shows high, resp. low effusivity values. In the right plot, we observe the opposite.

We then assumed that these coatings are laid over a substrate (semi-infinite layer) of effusivity b_1, i.e., the one at the right-edge of the coating. Thus, the effusivity is continuous up to the first derivative at the interface. The temperature response of the free surface of the coating when it is submitted to a modulated heat input of power density (amplitude) P and frequency f is represented in Fig. 3 (amplitude in left plot, phase in right plot). In the absence of heat losses, the front-surface temperature is given by:

$$\theta = P\frac{AZ+B}{CZ+D} \tag{26}$$

where $Z = \left(b_1\sqrt{p}\right)^{-1} = \left(b_1\sqrt{i2\pi f}\right)^{-1}$ is the thermal impedance of the homogeneous semi-infinite layer and A, B, C, D are the four entries of the coating quadrupole (while taking appropriately $\langle T \rangle$-form or $\langle \varphi \rangle$-form related expressions in Eq. (22)-(25)). The normalized amplitude reported in Fig. 3-left is $\left|\theta b_0 / P\xi_1\right|$. The green curves in both plots describe the behavior of a single homogeneous material of effusivity b_0 (reference case). Amplitude and phase are plotted vs. the non-dimensional frequency $f\xi_1^2$ (values in the range of 1 indicate a frequency match with the coating diffusion time). The results in Fig. 3 were validated against the classical staircase profile model (homogeneous quadrupole method [29]). As expected, the results provided by the standard method converge to the new ones when refining discretization, i.e., increasing the number of homogeneous sublayers. The error induced by the staircase approximation on the temperature amplitude and phase is reported in Table 1. We also reported the computing time necessary to obtain a set of 1000 frequency data with both methods. The benefit of the new method in terms of CPU time increases with the number of sublayers. For example, when compared to the finest discretization case, i.e., 100 sublayers, the computing time is divided by about 5 with the new method. One should however mention that this factor is reduced when less

frequency data are necessary, namely it drops to 2.4 when only 100 frequency data are computed. Anyway, not only is the standard method approximate, but in these cases it is also less rapid. In addition, it exposes the calculations to round-off errors when increasing the number of sublayers. The number of sublayers for which both methods are equivalent in terms of CPU time is 15, resp. 38, when the number of computed frequency data is 1000, resp. 100. When implementing the $\mathrm{sech}\left(\hat{\xi}\right)$-quadrupole, a significant amount of time is devoted to the evaluation of the two non-linear parameters ξ_c and τ, namely 5 ms. For the particular, albeit important case of $\mathrm{sech}\left(\hat{\xi}\right)$ profiles with horizontal end-slopes [28], empirical formulas can be found for evaluating this pair of parameters, which allow the non-linear solver to be bypassed and the corresponding CPU time to be reduced considerably. The previously mentioned numbers of sublayers for which both methods are equivalent in terms of CPU time (i.e., 15 and 38) are then both reduced to 12. It is not excluded that all of these figures can be improved by further optimizing the software.

In Fig. 3, as expected, with increasing frequency, the asymptotic amplitude trend and phase level are those of the reference case. Reciprocally, under vanishing frequency, they come close to those of the bulk material. In the intermediate regime, i.e., $f\xi_1^2$ between 0.01 and 100 (which is quite a wide range), notwithstanding the global $f^{-1/2}$ trend, the amplitude in Fig. 3-left follows an evolution that very roughly corresponds to the inverse of the effusivity profile. On the other hand, in Fig. 3-right, the phase evolution looks more complicated and its variations are less easy to interpret with respect to the known in-depth variations of effusivity. At first glance, one might assume that the phase contrast to the reference value -45° is loosely related with the derivative of the effusivity profile with respect to ξ.

Ultimately, the three groups of profiles show extremely different thermal behaviors, suggesting that the inversion of amplitude and phase data to characterize the graded profiles is likely to succeed. However, discriminating between the presently considered $\langle T \rangle$-form and $\langle \varphi \rangle$-form profiles will be unequally easy. The highest difficulty will be with the monotonically rising profiles (blue curves), since those are very close anyway.

Another way of representing the temperature amplitude $|\theta(f)|$ consists in multiplying it by $f^{1/2}$ to compensate for the general $f^{-1/2}$ trend and then taking the inverse. Indeed, computing $P/\left(|\theta(f)|\sqrt{2\pi f}\right)$ yields a frequency-dependent function that has the dimension of effusivity and whose asymptotic values are b_0 for $f \to \infty$ and $b(\xi \to \infty) = b_1$ for $f \to 0$. We may call this function "apparent effusivity": $b_{app}(f)$. Actually, the time-domain version of this "apparent effusivity" (i.e., as inferred from the pulse temperature response) was first presented in [32, 33] and it later found many applications in the field of photothermal measurements (see, e.g., [34-36]).

In the frequency domain, a frequency scan from high to low values yields "apparent effusivity" values that are expected to provide information on the *actual effusivity* values at progressively deeper levels. That $b_{app}(f)$ dispenses a perfect image of the effusivity profile $b(\xi)$, through a still-unknown relationship between f and SRDT ξ, is however a naive thought. Fig. 4 presents the (normalized by b_1) apparent effusivity curves related to all six $\mathrm{sech}(\hat{\xi})$ profiles in Fig. 1. First, the variations of the apparent effusivity are damped with respect to those of the true profiles (non-monotonic cases). The damping is particularly important for the profiles exhibiting an overshoot (red curves). Secondly, the relation between the ξ/ξ_1 -scale (in Fig. 1) and the frequency-scale $f\xi_1^{\,2}$ (in Fig. 4) is far from obvious; anyway it cannot be reduced to a mere $x \to 1/\sqrt{x}$ transformation. Therefore, the apparent effusivity curves should only be considered as a rough description of the actual effusivity profiles. More involved inversion procedures should be implemented to obtain a valuable description of these, which will be the subject of a future paper.

5.2 Synthesis of more elaborate profiles

More complex (solvable) profiles can be synthesized by joining several $\mathrm{sech}(\hat{\xi})$-type profiles. Thanks to their flexibility, one can manage to obtain synthetic profiles that are continuous at the nodes up to the first or even second derivative. Figure 5 is a collection of five such synthetic profiles incorporating up to ten $\mathrm{sech}(\hat{\xi})$-type elements (the profiles of $\sqrt{b(\xi)}/\sqrt{b_\infty}$ are represented vertically vs. ξ/ξ_{total}, where ξ_{total} is the SRDT of all of the graded part of the profile). They are backed by a homogeneous semi-infinite layer with effusivity b_∞. Intricate functions of this kind could be good candidates for modeling effusivity profiles encountered, for example, in natural or artificial soils.

The associated temperature response is obtained by first multiplying together the quadrupoles related to each $\mathrm{sech}(\hat{\xi})$-type element and then applying Eq. (26) by substituting the entries of the resulting "multilayer" quadrupole. The adiabatic temperature response (normalized amplitude and phase) at the free surface of the five synthetic profiles in Fig. 5 is reported in Fig. 6 (it was assumed that the input power is absorbed at the upper surface). The green curves describe the behavior of a homogeneous material of effusivity b_∞ (reference case) towards which all amplitude and phase curves tend under vanishing frequency. On the other side, the amplitude at asymptotically high frequency is conditioned by the effusivity value at the upper surface (inverse relationship). Therefore, in Fig. 6-left, at a normalized frequency of 100, the amplitude obtained with Effusivity Profiles No. 1 (cyan), No. 2 (black) and No. 5 (red) (the numbers refer to the synthetic profiles described in Fig. 5 from left to right) is very similar, whereas it is much higher than the one obtained with Effusivity Profiles No.

3 (blue) and No. 4 (magenta). The amplitude variations with decreasing frequency are inversely correlated with the in-depth evolution of the respective effusivity profiles. However, the deep effusivity variations have a progressively lower impact on the temperature amplitude, being hidden by the shallower variations. This would considerably hinder the reconstruction process of the deep part of the profiles, which is a well-known difficulty in thermal inversion (see, e.g., [9-11, 14, 16-19, 21]).

Let us underscore that the amplitude and phase curves in Fig. 6 are the *exact* thermal responses of the effusivity profiles represented in Fig. 5. These results show that there is no longer any difficulty in obtaining *exact temperature results* for arbitrarily complex effusivity profiles. From this perspective, the "high-level" quadrupoles related to $\mathrm{sech}\left(\hat{\xi}\right)$-type elementary profiles can be considered as sophisticated analytical Meccano pieces (as opposed to the classical straight profiles). In addition to this aim, we have sought, through the choice of the geometric forms represented, to offer a mnemonic means to remember the name of the functions that are the basis of this technique: the $\mathrm{sech}\left(\hat{\xi}\right)$ profiles ([sek ksi hæt] = [seksi hæt]). For this purpose, the synthetic profiles in Fig. 5 have been superimposed in Fig. 7.

6 Discussion and extension to other transfer equations (Maxwell's equations)

The previous results highlighted the advantages of exploiting the $\mathrm{sech}\left(\hat{\xi}\right)$-type profile concept for solving the *direct* thermal problem in graded media. The dynamic temperature data referred to the frequency domain. To obtain, instead, the transient data corresponding to a pulsed excitation, one should still perform an inverse Laplace transformation on the temperature expression in Eq. (26) (whilst involving the Laplace variable p). This is easily and efficiently performed numerically by the De Hoog method [30, 37].

In the near future, we will tackle the *inverse* problem, namely the identification of an effusivity profile (through a $\mathrm{sech}\left(\hat{\xi}\right)$-type profile description) from the pulsed or modulated photothermal data measured on the outer surface of a (presumably) continuously heterogeneous material. The problem could be addressed sequentially as follows. As a first step, one could solve the following problem: which $\mathrm{sech}\left(\hat{\xi}\right)$-type profile best corresponds to the temperature observations? This essentially reduces to a five-parameter identification problem: it is necessary to evaluate the total diffusion time ξ_1 and the four boundary specifications regarding the $\mathrm{sech}\left(\hat{\xi}\right)$-type profile (effusivity value and effusivity slope at both ends of the material). The two options, the $\langle T \rangle$-form or $\langle \varphi \rangle$-form profile, should be considered separately and the one leading to the best fit should be retained. Next, if this result is not satisfactory, the ξ-domain should be split into two parts and a pair of connected $\mathrm{sech}\left(\hat{\xi}\right)$-type profiles should be introduced. Different avenues are then open, depending on the constraints applied on the junction

node: the synthetic profile could be either simply continuous, or continuous up to the first derivative or the second derivative. In addition, four combinations are available, depending on the form, $\langle T \rangle$ or $\langle \varphi \rangle$, chosen for the two layers. Furthermore, one could recursively subdivide the ξ-domain. However, most probably, a small number of $\mathrm{sech}\left(\hat{\xi}\right)$-type profiles will be satisfactory, because of their great flexibility. If needed, one could also add a semi-infinite profile of $\tanh(\xi)$-type to model the deep monotonous evolution of effusivity, as illustrated in Ref. 26. In the end, fairly complex and arbitrarily steep profiles could be well modeled by requiring the adjustment of a relatively small number of parameters, which is a good point when striving for parsimonious inversion with no strong correlation between parameters. The PROFIDT method and the related products, among them the powerful $\mathrm{sech}\left(\hat{\xi}\right)$-type profiles, are not restricted to the heat equation. They can also be applied to wave equations used to model plane wave propagation in 1D graded media, like in optics (Maxwell's equations), in acoustics (acoustic waves and shear waves) and in heterogeneous transmission lines (telegraph equation). The adaptation of the PROFIDT method to Maxwell's equations in lossless materials with graded permittivity and permeability was performed in [28]. Optical materials with a graded refractive-index present a subcase.

There are actually interesting equivalences with the heat transfer problem. Roughly speaking, there is a close connection between, on one side, the effusivity, the SRDT, $\langle T \rangle$-form and $\langle \varphi \rangle$-form profiles, and on the other side the (effective) refractive index, the optical thickness, $\langle E \rangle$-form and $\langle H \rangle$-form profiles, where E and H stand for the electric and magnetic fields. In essence, the $\langle T \rangle$-form quadrupole in Eq. (22), (24) is the same as the $\langle E \rangle$-form quadrupole; it is simply necessary to perform the following change $p \leftrightarrow -k_0^2$, where k_0 is the wavenumber in vacuum of the light wave (the quadrupole transformation from $\langle E \rangle$-form to $\langle H \rangle$-form is however not the same as between $\langle T \rangle$-form and $\langle \varphi \rangle$-form in Eq. (25); it actually reduces to a two-step circular permutation, see [28]).

The $s(\xi)$ profiles are strictly the same for both problems, making the $\mathrm{sech}\left(\hat{\xi}\right)$-type profiles of the same (great) interest for both. As an example, a multiplicity of $\mathrm{sech}\left(\hat{\xi}\right)$-type profiles with zero end-slopes were joined calculating calculate the exact reflectance/transmittance spectra of locally-periodic refractive-index profiles encountered in rugate filters, Bragg gratings or in chirped mirrors [28].

More illustrations of the power of the $\mathrm{sech}\left(\hat{\xi}\right)$-type profiles for diffusion and wave modeling in continuously heterogeneous media, both for direct and inverse problems, are expected in the future.

7 Conclusion

A high-level thermal quadrupole has been proposed for modeling continuously heterogeneous materials. It corresponds to a double class of effusivity profiles, the so-called $\mathrm{sech}\left(\hat{\xi}\right)$-type profiles, of either $\langle T \rangle$-form or $\langle \varphi \rangle$-form. They have recently been shown to lead to an exact analytical solution of the heat equation, based on Liouville and Darboux transformations. These profiles of finite thickness are defined by their characteristic diffusion time, and by four other parameters that can be evaluated once the effusivity and its slope are specified at both ends of the layer. The interest of the $\mathrm{sech}\left(\hat{\xi}\right)$-type profiles lies in their great flexibility and in the fact that the quadrupole entries are in closed-form and only involve elementary functions. This high-level quadrupole outperforms the standard homogeneous quadrupole method in terms of computing time when more than a few tens of sublayers are necessary for the profile discretization, which may be necessary to accurately model steep variations in effusivity. Multiplying $\mathrm{sech}\left(\hat{\xi}\right)$-type quadrupoles by each other offers the possibility of modeling the response of a smooth effusivity profile of virtually any shape.

With minimal modifications, we obtain the expression of an analytical transfer matrix suitable for modeling wave propagation in graded media as well as for optics in dielectrics presenting a gradual evolution of the refractive index.

References

1. R.M. Mahamood, E.T. Akinlabi, *Functionally Graded Materials*, (Springer, 2017).
2. H.S. Carslaw, J.C. Jaeger, *Conduction of heat in solids*, (Oxford Univ. Press, 1959), pp. 15.412-15.415.
3. A.K.S. Thakur, Lett. Heat Mass Transfer **9**, 385 (1982)
4. W.J. Massman, Soil Sci. **155**, 331 (1993)
5. J. Fivez, C. Glorieux, J. Appl. Phys. **108**, 103506 (2010)
6. A. Sutradhar, G. H. Paulino, Comput. Methods Appl. Mech. Engrg. **193**, 4511 (2004)
7. T. Ishiguro, A. Makino, N. Araki, N. Noda, Int. J. of Thermophys. **14**, 101 (1993)
8. J.-C. Krapez, S. Profice, Proc. SFT 2011, F. Bataille and G. Flamant eds., Editions SFT (2011), p. 293
9. J. J. Alvarado-Leaños, J. Ordonez-Miranda, J. J. Alvarado-Gil, Int. J. of Thermophys. **34**, 1457 (2013)
10. C. Glorieux, J. Fivez, J. Thoen, J. Appl. Phys. **73**, 684 (1993)
11. R. Celorrio, E. Apiñaniz, A. Mendioroz, A. Salazar, A. Mandelis, J. Appl. Phys. **107**, 083519 (2010)
12. M.S. Sodha, A. Sengupta, R.L. Sawhney, Int. J. Energy Research **17**, 121 (1993)
13. K. Friedrich, U. Seidel, H. G. Walther, W. Karpen, G. Busse, Res. in Nondestr. Eval., **5**, 31 (1993)

14. T.T.N. Lan, U. Seidel, H.G. Walther, J. Appl. Phys. **77**, 4739 (1995)
15. P. Grossel, F. Depasse, Int. J. Thermal Sci. **50**, 2078 (2011)
16. V. Gusev, T. Velinov, K. Bransalov, Semicond. Sci Technol. **4**, 20 (1989)
17. P. Grossel, F. Depasse, N. Trannoy, J. Phys. III **7**, 13 (1997)
18. R. Li Voti, M. Bertolotti, C. Sibilia, Adv. in Signal Processing for NDE of Materials (1997)
19. J.-C. Krapez, J. Appl. Phys. **87**, 4514 (2000)
20. A.K.S. Thakur, M. Musa Momoh, Energy Convers. Mgmt. **23**, 131 (1983)
21. A. Mandelis, F. Funak, M. Munidasa, J. Appl. Phys. **80**, 5570 (1996)
22. R.M. Cotta, B.P. Cotta, C.P. Naveira-Cotta, G. Cotta Pereira, Int. J. Thermal Sci. **49**, 1510 (2010)
23. K.V. Khmelnytskaya, I. Serroukh, Math. Meth. Appl. Sci. **11**, 065707 (2013)
24. J. Fivez, J. Thoen, J. Appl. Phys. **79**, 2225 (1996)
25. E. Varley, B. Seymour, Studies in Appl. Math. **78**, 183 (1988)
26. J.-C. Krapez, Int. J. Heat Mass Transfer **99**, 485 (2016)
27. J.-C. Krapez, J. Phys.: Conf. Ser. **745**, 032059 (2016)
28. J.-C. Krapez, J. Modern Optics **64**, 1988 (2017)
29. D. Maillet, S. André, J.-C. Batsale, A. Degiovanni, C. Moyne, *Thermal Quadrupoles: Solving the Heat Equation through Integral Transforms*, (J. Wiley & Sons, New-York, 2000)
30. J.-C. Krapez, E. Dohou, Int. J. Therm. Sci. **81**, 38 (2014)
31. D. Zwillinger, *Handbook of differential equations* (Academic Press, 1997)
32. J.-C. Krapez, *Mesure de l'effusivité thermique par la méthode flash. Application aux matériaux stratifiés*, DEA, ECP, 1984.
33. D. L. Balageas, J. C. Krapez, P. Cielo, J. Appl. Phys. **59** 348-357 (1986)
34. A. Kusiak, J.Martan, J. L. Battaglia, R. Daniel, Thermochimica acta, **556**, 1-5 (2013)
35. V.Vavilov, S. Marinetti, Y. Pan, A. Chulkov, Polymer Testing, **54**, 270-280 (2016)
36. J. G. Sun, J. of Heat Transfer, **138** 112004 (2016)
37. J. Toutain, J. -L. Battaglia, C. Pradere, J. Pailhes, A. Kusiak, W. Aregba, J.-C. Batsale, J. of Heat Transfer **133**, 044504 (2011)

Table 1

Method		CPU time (ms)	Ratio of CPU times (standard/new)	Max. error on temperature amplitude (%)	Max. error on temperature phase (°)
Standard quadrupoles	N=25 layers	$0.1^{a} + 64^{b} \approx 64$	1.5	5.8	1.4
	N=50 layers	$0.1^{a} + 111^{b} \approx 110$	2.6	1.7	0.7
	N=100 layers	$0.12^{a} + 209^{b} \approx 209$	4.9	0.4	0.2
$\mathrm{sech}\left(\hat{\xi}\right)$ quadrupole		$5^{c} + 37^{d} = 42$		-	-

[a] time to discretize the profile
[b] time to calculate the N quadrupoles, perform their multiplication and infer the temperature
[c] time to evaluate the profile parameters ξ_c and τ
[d] time to calculate the $\mathrm{sech}\left(\hat{\xi}\right)$ quadrupole and infer the temperature

Computation time for the standard staircase quadrupole method, depending on the number of homogeneous sublayers, and for the $\mathrm{sech}\left(\hat{\xi}\right)$-quadrupole method (Intel Xeon, 2.8 GHz, 64bits processor; Matlab code, 1000 frequency data). The two rightmost columns contain the maximum error on temperature amplitude and phase when using the standard method.

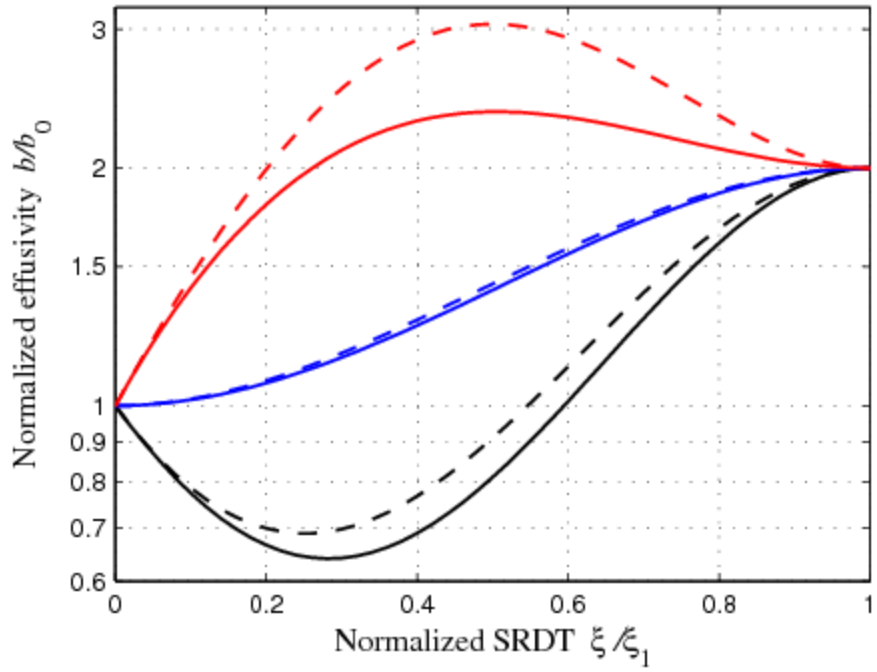

Fig. 1 Effusivity profiles of $\mathrm{sech}(\hat{\xi})$–type with various boundary specifications. The effusivity $b(\xi)$ is normalized by the left-edge value b_0. The profiles are plotted against the normalized SRDT (square root of the diffusion time) ξ/ξ_1, where ξ_1 is the SRDT of the graded layer. The profiles of $\langle T \rangle$-form are represented by continuous lines, those of $\langle \varphi \rangle$-form are represented by dashed lines. The right-to-left effusivity ratio b_1/b_0 is 2. Three values are considered for the left-end (dimensionless) derivative $\xi_1(b')_0/b_0$: -1.5 (black), 0 (blue) and +2 (red). The right-end derivative is 0 for all six cases.

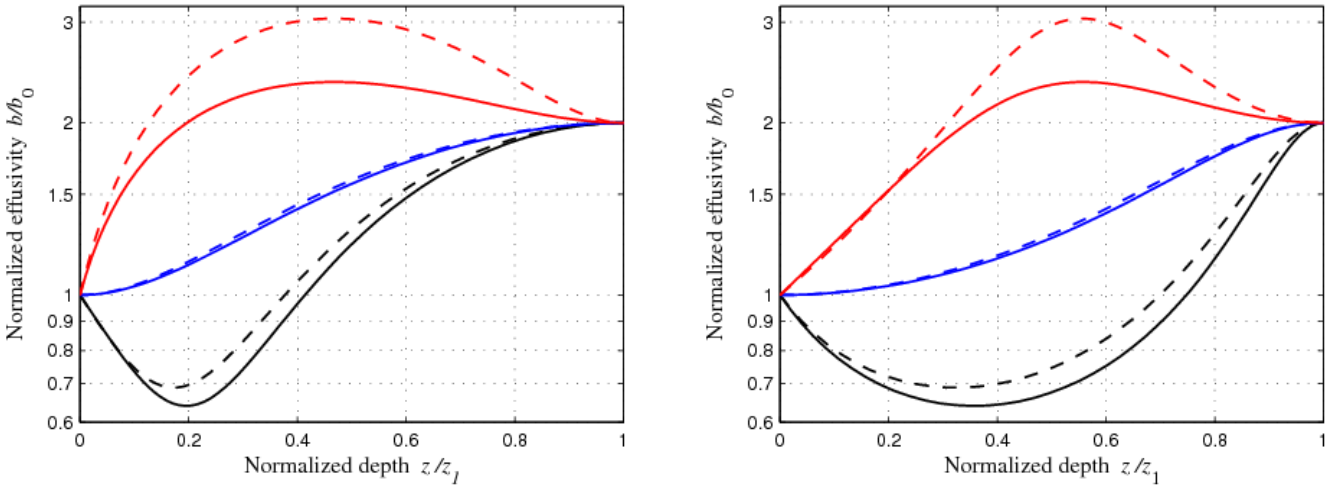

Fig. 2 Effusivity profiles of Fig. 1 represented in the physical-depth space, i.e., vs. z/z_1 where z is the distance from the left boundary and z_1 is the layer thickness. Two cases were considered for the $\xi \to z$ (inverse-Liouville) transformation. In the left plot, the underlying assumption is that the volumetric heat capacity is constant in the graded layer. In the right plot, heat conductivity was assumed to be constant.

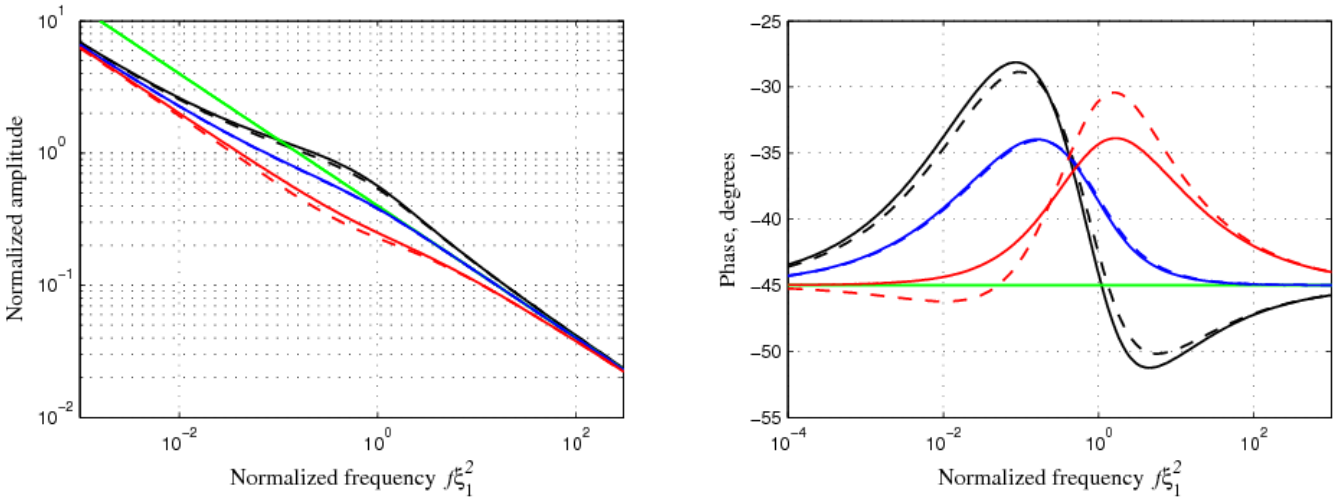

Fig. 3 Temperature response (on the left is the normalized amplitude –see the text– and on the right is the phase) of the profiles drawn in Fig. 1 and Fig. 2, when laid over a semi-infinite layer of effusivity b_1 and submitted at the left boundary $\xi = 0$ to a modulated heat input of frequency f. The amplitude and phase are plotted vs. the normalized frequency $f\xi_1^2$. Same colors as in Fig. 1 and Fig. 2. The additional green line corresponds to the response of a homogeneous semi-infinite material whose effusivity is equal to the surface effusivity of the graded profiles, b_0.

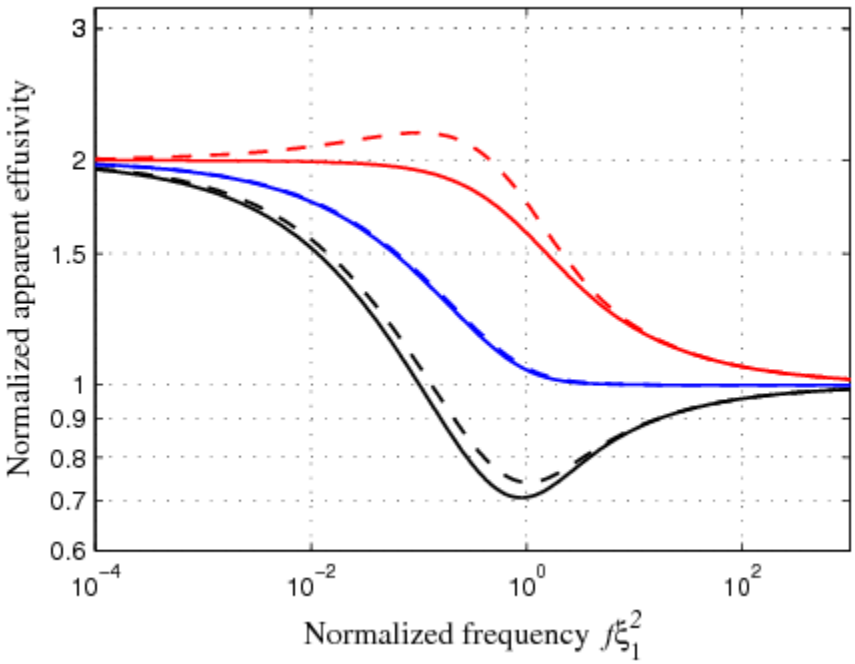

Fig. 4 Same as in Fig. 3 for the (normalized) apparent effusivity, which corresponds to the ratio between the amplitude of the homogeneous (reference) material and the amplitude of the graded material. This apparent effusivity is a frequency function; it is here plotted vs. the normalized frequency $f\xi_1^2$.

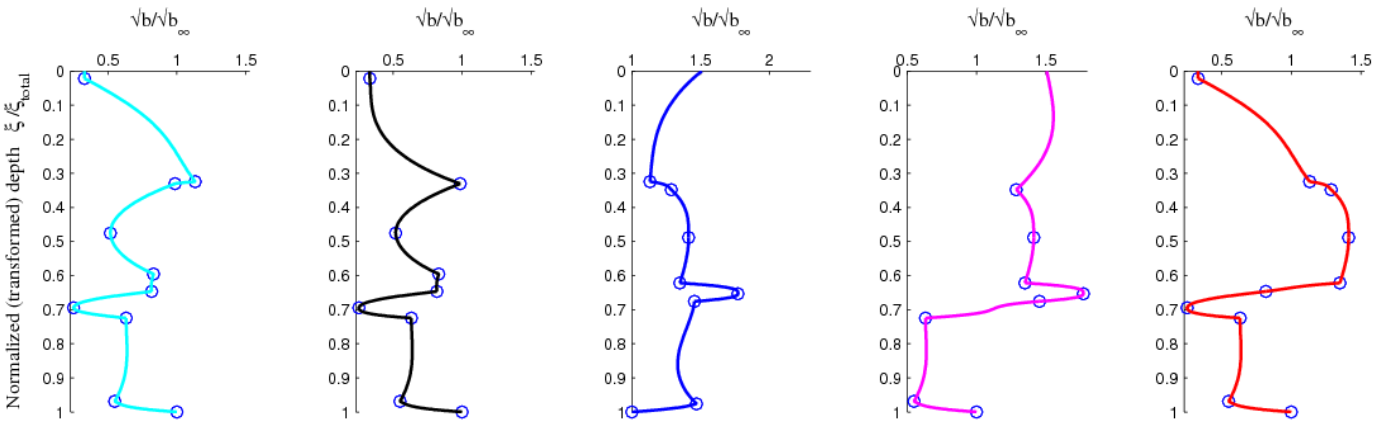

Fig. 5 A series of five composite effusivity profiles, obtained by joining up to ten $\mathrm{sech}(\hat{\xi})$–type profiles. The vertical profiles of the square root of effusivity (normalized by the bulk value) is plotted vs. the normalized SRDT (square root of the diffusion time) ξ/ξ_{total}, where ξ_{total} is the SRDT of the whole graded profile. Blue circles indicate the connection nodes.

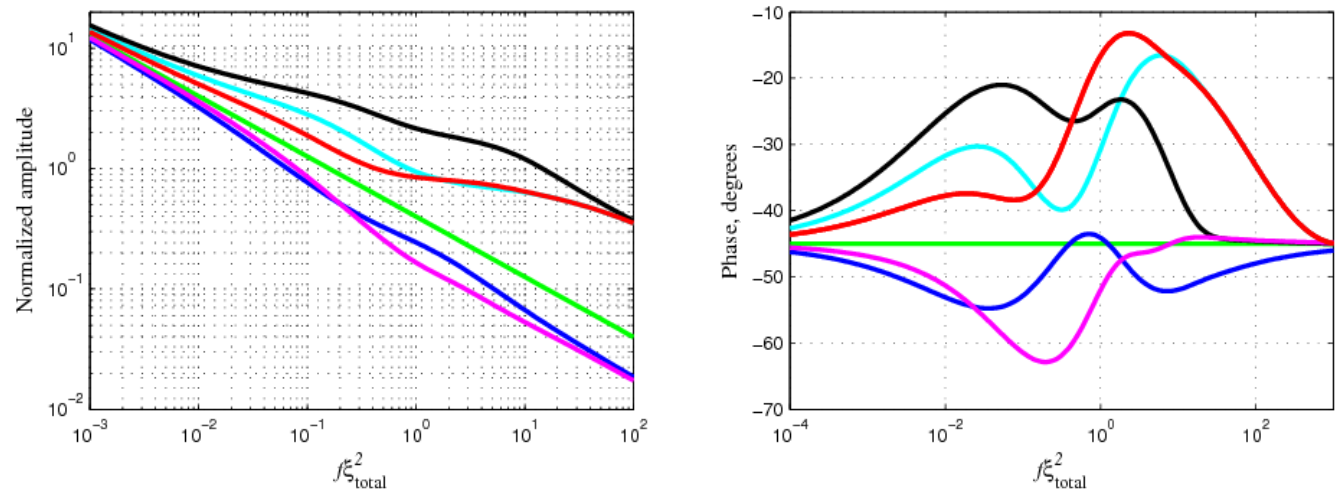

Fig. 6 Temperature response (left: normalized amplitude, right: phase) of the profiles drawn in Fig. 5, while laid over a semi-infinite layer of effusivity b_∞ and submitted at the top boundary $\xi = 0$ to a modulated heat input of frequency f. The amplitude and phase are plotted vs. the normalized frequency $f\xi_{tot}^2$ (for the colors, refer to Fig. 5). The additional green lines correspond to the response of a homogeneous semi-infinite material whose effusivity is equal to the bulk effusivity of the graded profiles, i.e., b_∞.

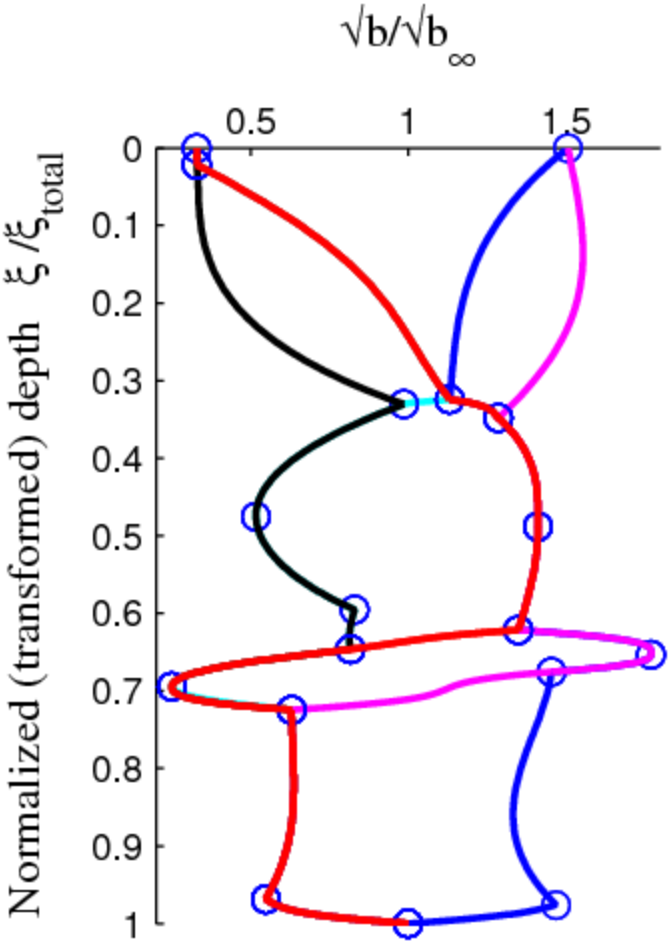

Fig. 7 Superposition of the five synthetic profiles from Fig. 5. In addition to its mnemonic power, this figure intends to show the large variety of shapes that can be built from the basis of $\mathrm{sech}\left(\hat{\xi}\right)$ ([seksi hæt]) profiles.